



# Disruption of the standard kinetochore in holocentric *Cuscuta* species

Pavel Neumann<sup>a,1</sup> , Ludmila Oliveira<sup>a</sup> , Tae-Soo Jang<sup>a,b</sup> , Petr Novák<sup>a</sup> , Andrea Koblížková<sup>a</sup> , Veit Schubert<sup>c</sup> , Andreas Houben<sup>c</sup> , and Jiří Macas<sup>a</sup>

Edited by Steven Henikoff, Fred Hutchinson Cancer Research Center, Seattle, WA; received January 17, 2023; accepted April 17, 2023

The segregation of chromosomes depends on the centromere. Most species are monocentric, with the centromere restricted to a single region per chromosome. In some organisms, the monocentric organization changed to holocentric, in which the centromere activity is distributed over the entire chromosome length. However, the causes and consequences of this transition are poorly understood. Here, we show that the transition in the genus *Cuscuta* was associated with dramatic changes in the kinetochore, a protein complex that mediates the attachment of chromosomes to microtubules. We found that in holocentric *Cuscuta* species, the *KNL2* genes were lost; the *CENP-C*, *KNL1*, and *ZWINT1* genes were truncated; the centromeric localization of *CENH3*, *CENP-C*, *KNL1*, *MIS12*, and *NDC80* proteins was disrupted; and the spindle assembly checkpoint (SAC) degenerated. Our results demonstrate that holocentric *Cuscuta* species lost the ability to form a standard kinetochore and do not employ SAC to control the attachment of microtubules to chromosomes.

kinetochore | centromere | holocentric | monocentric | *Cuscuta*

Faithful segregation of chromosomes during mitosis and meiosis depends on the centromere, a chromosomal domain that facilitates the attachment of chromosomes to spindle microtubules. In monocentric chromosomes, the centromere is localized at a single site per chromosome, which is morphologically discernible as a primary constriction. Holocentric chromosomes, on the contrary, lack this primary constriction and instead have the centromere domains distributed along almost the entire chromosome length. Holocentricity evolved from monocentric organization independently several times during the evolution of both plants and animals (1); however, the causes of the transitions are still enigmatic. This is primarily because only a few holocentric species have been studied so far and because most groups of holocentric species evolved from the monocentric ancestors a long time ago, making the factors involved in the transition elusive.

In most species, the centromere is epigenetically determined by the presence of *CENH3*, a centromere-specific variant of histone H3 that replaces the canonical H3 histones in centromeric nucleosomes (2). At the same time, *CENH3* serves as the basis for the kinetochore, a complex multiprotein structure that mediates the connection between centromeric chromatin and the microtubules of the mitotic spindle in most species. The backbone of the kinetochore consists of the constitutive centromere-associated network (CCAN), which connects the kinetochore with centromeric chromatin, and the KMN network, which constitutes an interface toward spindle microtubules (3, 4). The function of the kinetochore is regulated by additional proteins, the most studied of which belong to the spindle assembly checkpoint (SAC) (5, 6) and the chromosome passenger complex (CPC) (7–9).

The role of *CENH3* in centromere determination predicts that the transition from monocentric to holocentric centromere organization requires the formation of *CENH3*-containing domains along entire chromosomes. Indeed, in the few holocentric species studied to date, *CENH3* is typically localized along the entire poleward surface of each chromatid where microtubules attach (10, 11). An exception are holocentric insects that lack *CENH3* and use an alternative pathway of kinetochore assembly that depends on *CENP-T* protein (12–14).

Recently, we identified the first exception in plants, in *Cuscuta europaea*, which belongs to the holocentric subgenus *Cuscuta* of the parasitic plant genus *Cuscuta* (Convolvulaceae) (15). In this species, the chromosomes restrict *CENH3* to only one to three heterochromatin bands, despite being attached to the mitotic spindle along their entire length. This suggests that *CENH3* has either lost its centromere function in this species or acts in parallel with an additional *CENH3*-independent mechanism of kinetochore assembly. Since monocentric relatives of *C. europaea* from the sister subgenus, *Grammica*, and the more distant subgenus, *Monogynella*, have *CENH3* localized specifically in primary constrictions (16), it is plausible that the peculiar *CENH3* localization in *C. europaea* resulted

## Significance

Segregation of chromosomes depends on the centromere and the kinetochore, which mediates its connection to spindle microtubules. In contrast to monocentric chromosomes with a single centromere domain, holocentric chromosomes, which evolved from monocentric ones independently several times in both animals and plants, usually have hundreds of centromere units distributed along the entire chromosome length. Here, we report that holocentric chromosomes in the parasitic plants of the genus *Cuscuta* divide properly during mitosis despite dramatic changes in their kinetochore composition, suggesting a unique mechanism of chromosome segregation. Our results, together with recent discoveries in other species, suggest that centromere determination and kinetochore composition are remarkably plastic in holocentric organisms and thus may provide important insights into the principles of chromosome segregation.

**Preprint Servers:** The manuscript has been deposited in the bioRxiv preprint server (<https://www.biorxiv.org/content/10.1101/2023.01.04.522735v1>) and is made available under a CC-BY-NC-ND 4.0 International license. The authors declare no competing interest.

This article is a PNAS Direct Submission.

Copyright © 2023 the Author(s). Published by PNAS. This open access article is distributed under Creative Commons Attribution-NonCommercial-NoDerivatives License 4.0 (CC BY-NC-ND).

<sup>1</sup>To whom correspondence may be addressed. Email: neumann@umbr.cas.cz.

This article contains supporting information online at <https://www.pnas.org/lookup/suppl/doi:10.1073/pnas.2300877120/-DCSupplemental>.

Published May 16, 2023.

from changes in kinetochore assembly that were linked to the transition to holocentricity in the subgenus *Cuscuta*. However, how kinetochore assembly has changed and whether these changes are related to the transition to holocentricity remain unknown.

In this study, we addressed these questions by comparing the repertoire of major structural and regulatory kinetochore proteins and their chromosomal localization between two *Cuscuta* species from the holocentric subgenus *Cuscuta* (*C. europaea* and *C. epithymum*), two monocentric *Cuscuta* species from the sister subgenus *Grammica* (*C. australis* and *C. campestris*), and *Ipomoea nil*, which was included as an outgroup Convolvulaceae species. To obtain high-quality data for gene identification in the two holocentric *Cuscuta* species, we sequenced both their genomes and transcriptomes. The chromosomal localization of kinetochore proteins was determined using antibodies developed against key proteins representing different subcomponents of the kinetochore. Comparison of the results between monocentric and holocentric species allowed us to uncover an unprecedented level of changes that occurred specifically in the holocentric species and thus likely played an important role in the transition to holocentricity in *Cuscuta*.

## Results

**Transition to Holocentricity in *Cuscuta* Was Associated with Massive Changes in Kinetochore Protein Genes.** Sequencing of the holocentric species *C. europaea* and *C. epithymum* resulted in genome assemblies of 975.8 Mb (N50 = 17.9 Mb) and 997 Mb (N50 = 3.3 Mb), respectively (SI Appendix, Supporting text and Table S1). The completeness of gene space and quality of gene prediction were assessed using BUSCO and were comparable to genome assemblies previously published for the monocentric *Cuscuta* relatives *C. australis* and *C. campestris* (SI Appendix, Fig. S1). The quality of gene prediction in the genome assembly was also verified by the independent assembly of the transcriptomes, which showed similar results following BUSCO analysis (SI Appendix, Table S2). To identify kinetochore protein sequences in the species selected for this study, we created a sequence database of 29 structural and regulatory kinetochore proteins known in plants. First, we used the database as a query for blastp searches to identify homologous protein sequences in the monocentric species *C. australis*, *C. campestris*, and *Ipomoea nil*. The identified sequences were manually verified and corrected when needed and added to the database to improve its sensitivity for homologous protein recognition. The improved database was then used for blastp searches in the two holocentric *Cuscuta* species. Comparison of the identified kinetochore protein genes revealed that all the 29 tested genes are present and mostly intact in the monocentric species, whereas in the holocentric species, some of the genes are either absent, significantly truncated, or duplicated accompanied by a higher rate of sequence divergence (Fig. 1A, SI Appendix, Table S3, and Dataset S1). Transcriptome data analysis revealed that the intact and truncated genes identified in holocentric *Cuscuta* species are transcribed.

The lost genes included both eudicotyledonous plant homologs of *KNL2*, referred to as  $\alpha$ *KNL2* and  $\beta$ *KNL2* (25), and four of the eight spindle assembly checkpoint (SAC) genes, namely, *BMF1*, *BMF2*, *BMF3*, and *MAD2* (Fig. 1A). Their absence was in all cases confirmed by comparison of genomic loci possessing these genes in *C. australis* with the orthologous loci in *C. europaea* and *C. epithymum* (SI Appendix, Figs. S2–S4), as well as by their absence in genome-independent transcriptome assemblies. The only exception was *BMF1* whose transcriptionally inactive fragment remains in *C. epithymum* (SI Appendix, Fig. S3). Large gene truncations

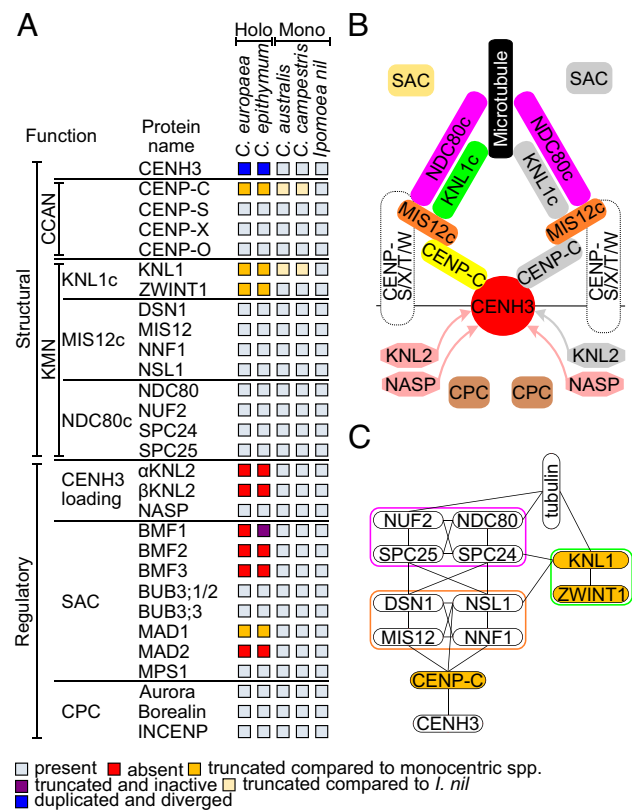
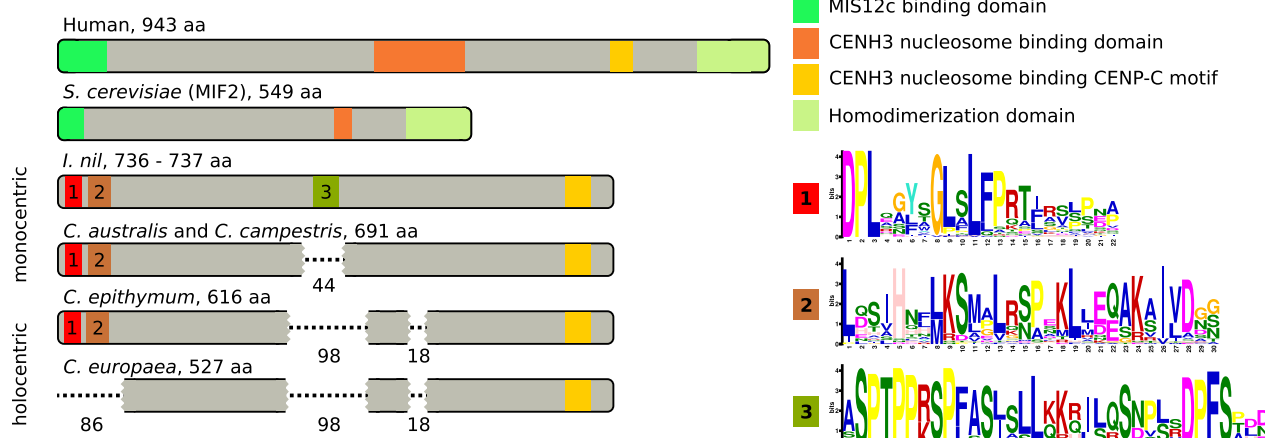


**Fig. 1.** The repertoire of structural and regulatory kinetochore proteins analyzed in this study. (A) Results of the survey of the protein sequences. (B) Simplified schematic illustration of kinetochore structure (3, 4). Proteins or complexes containing proteins that have been truncated or lost in holocentric *Cuscuta* species are highlighted in gray on the right. Centromeric chromatin is determined by the presence of CENH3. The deposition of CENH3 in plants depends on the KNL2 and NASP proteins. The outer kinetochore consists of the KMN network, which includes three subcomplexes, KNL1c, MIS12c, and NDC80c. The connection between centromeric chromatin and the KMN network is mediated by CENP-C. Some metazoan species have an alternative pathway of kinetochore assembly based on CENP-T. CENP-T forms a complex with CENP-S, CENP-X, and CENP-W and also interacts with NDC80c and MIS12c (12, 17). Because the plant homologs of CENP-T are not known, it is not clear whether the CENP-T pathway also exists in plants. The precise spatiotemporal and orderly progression of mitosis is ensured by the activity of regulatory kinetochore proteins belonging to the spindle assembly checkpoint (SAC) and the chromosome passenger complex (CPC). The SAC monitors the state of chromosome attachment to spindle microtubules and prevents the transition from metaphase to anaphase until all sister chromatids are attached to microtubules (6). The CPC is involved in mitotic checkpoint activity, destabilizes improperly attached spindle microtubules, and promotes axial shortening of chromosome arms during anaphase (7–9). (C) Schematic illustration of the interactions between the proteins forming the CENP-C pathway of kinetochore assembly. Proteins truncated in holocentric *Cuscuta* species are highlighted in orange. The interactions were drawn based on findings in yeast and humans (18–24) but likely also occur in plants.

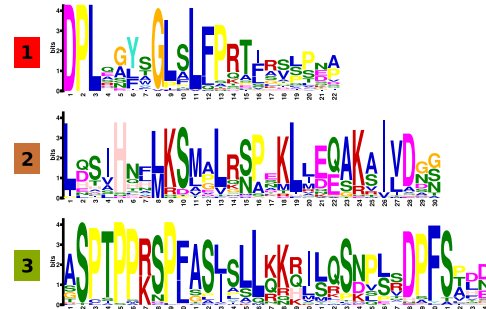
took place in three structural kinetochore protein genes, including *CENP-C*, *KNL1*, and *ZWINT1*, and the SAC gene *MAD1* (Figs. 2 and 3 and SI Appendix, Figs. S5 and S6). Finally, the *CENH3* gene in holocentric species was found to have duplicated once in the common ancestor of *C. europaea* and *C. epithymum*, and once independently in each of the two species. The diversification of the duplicated *CENH3* genes in holocentric species resulted in considerably higher protein sequence variability for *CENH3* compared with monocentric *Grammica* species, suggesting that they evolved more rapidly (SI Appendix, Figs. S7–S10).

Given the function of proteins that are either missing or truncated, the changes could have affected kinetochore assembly and function at multiple levels, from *CENH3* loading (absence of *KNL2*) and kinetochore assembly (truncation of *CENP-C*,

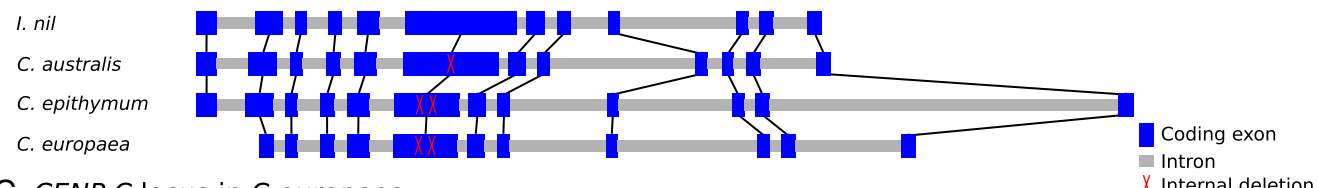
## A CENP-C structure



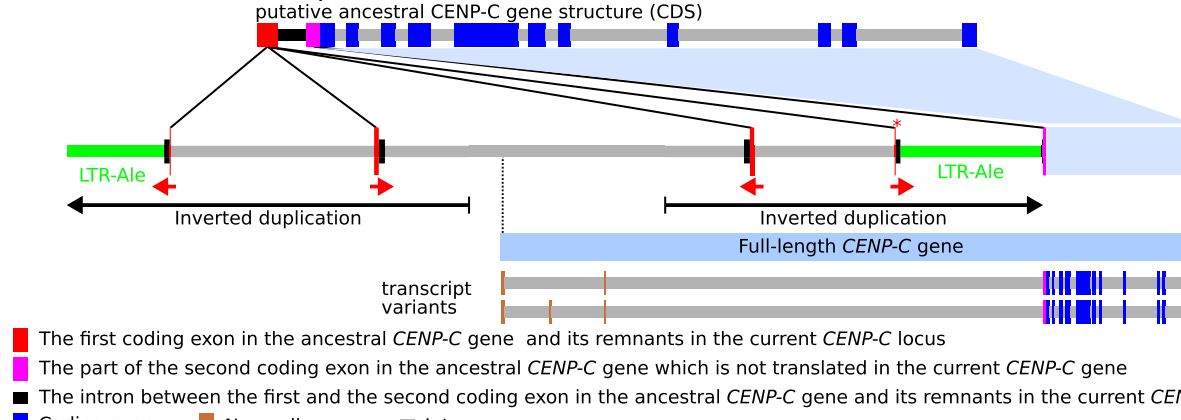
MIS12c binding domain  
CENH3 nucleosome binding domain  
CENH3 nucleosome binding CENP-C motif  
Homodimerization domain



## B Comparison of CDS exon / intron structure of CENP-C genes



## C CENP-C locus in *C. europaea*



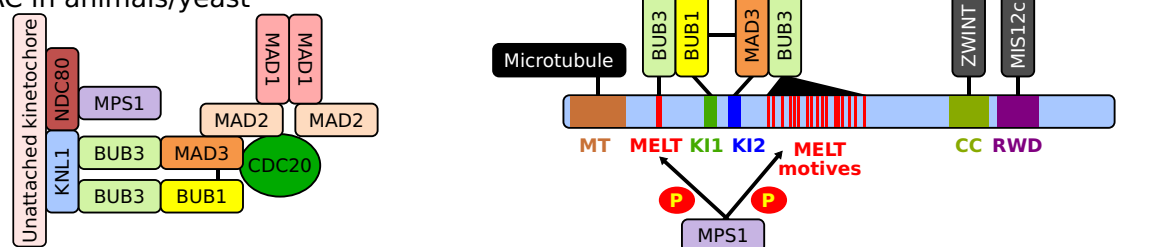
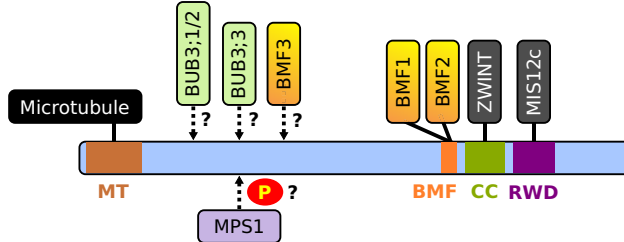
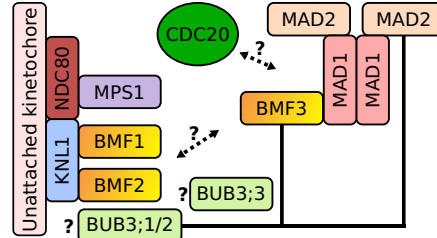
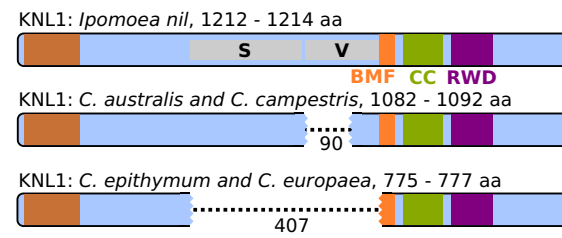
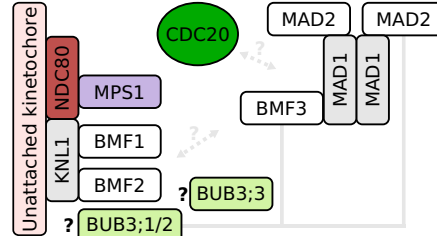
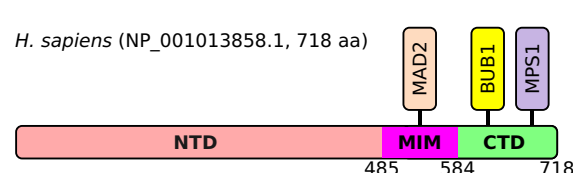
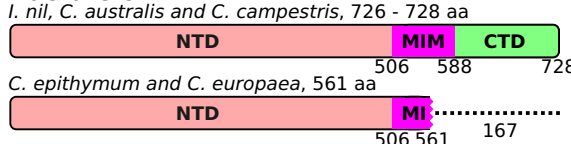
- The first coding exon in the ancestral CENP-C gene and its remnants in the current CENP-C locus
- The part of the second coding exon in the ancestral CENP-C gene which is not translated in the current CENP-C gene
- The intron between the first and the second coding exon in the ancestral CENP-C gene and its remnants in the current CENP-C locus
- Coding exon   ■ Noncoding exon   ■ Intron

**Fig. 2.** Truncation of CENP-C in *Cuscuta* species. (A) Comparison of domain structure between human, *Saccharomyces cerevisiae*, and monocentric and holocentric Convolvulaceae species. Human and yeast CENP-C sequences are divergent, but the positions of the functional domains are conserved (24, 26). Compared with *I. nil*, CENP-C is truncated in both monocentric and holocentric *Cuscuta* species, but with more extensive truncations in the latter species (the missing parts are shown as dashed lines, and the numbers below indicate their length). The N-terminal truncation in *C. europaea* and the internal truncations in all *Cuscuta* species resulted in the loss of domains recognized by MEME as conserved in dicotyledonous plants, suggesting possible functional significance. The sequence logos of these domains are shown on the Right. (B) Comparison of CDS exon-intron structure of CENP-C genes. The exon-intron structure is conserved in all Convolvulaceae species (the orthologous exons are connected with black lines). The internal truncations of CENP-C proteins in *Cuscuta* species are due to deletions in the sixth coding exon. (C) Schematic illustration of the CENP-C gene locus in *C. europaea*. The current CENP-C locus is compared with the putative ancestral CENP-C gene structure (Top), which was reconstructed by adding the missing region from *C. epithymum*. The original CENP-C gene gradually changed by a short inverted duplication of the first coding exon and part of the following intron (red arrows), a partial deletion in the first coding exon that remained in the correct orientation (marked with a red asterisk), the insertion of the Ty1/Copia LTR retrotransposon Ale (green), and a large inverted duplication (black arrows). The remnants of the first ancestral coding exon became part of the intron. The second ancestral coding exon was retained and became the first coding exon of the gene in present-day *C. europaea*.

KNL1, and ZWINT1), to regulation of its function (absence of several key proteins of SAC) (Fig. 1 B and C).

**CENH3 Histones Do Not Show a Holocentric-Like Distribution in Holocentric *Cuscuta* Species.** Since KNL2 is essential for the proper loading of CENH3 to centromeres (25, 33–35), the loss of both  $\alpha$ KNL2 and  $\beta$ KNL2 in holocentric *Cuscuta* species is likely to have a serious impact on CENH3 localization. On holocentric chromosomes, CENH3 is expected to specifically localize along the poleward side of each chromatid. In contrast to this expectation, we have previously shown that CENH3 occurs in all but one prominent transversal heterochromatin band in *C.*

*europaea* and that CENH3 distribution does not correlate with the distribution of mitotic spindle attachment sites detected with antibodies against  $\alpha$ -tubulin (15 and Fig. 4 A and B). To determine the localization of CENH3 in *C. epithymum*, we developed two antibodies against different N-terminal sequence variants of the proteins. Although the antibodies were made to recognize all CENH3 protein sequence variants present in the tested plant, neither of them produced a signal on chromosomes and nuclei that could be distinguished from the background (*SI Appendix*, Figs. S11, S12 A and B, and S13). On the contrary, both antibodies developed for *C. epithymum* detected CENH3 in the heterochromatin domains in *C. europaea* (*SI Appendix*, Fig. S11

**A SAC in animals/yeast****B Domain structure similarity of BUB1/MAD3 FAMILY proteins animals/yeast****C SAC in plants****D SAC in holocentric *Cuscuta* species****E Structure of MAD1**KNL1: *Ipomoea nil*, 1212 - 1214 aa

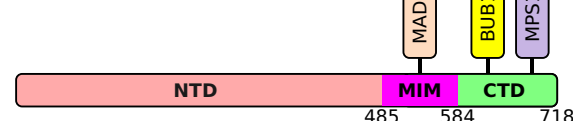
S V BMF CC RWD

KNL1: *C. australis* and *C. campestris*, 1082 - 1092 aa

90

KNL1: *C. epithymum* and *C. europaea*, 775 - 777 aa

407

*H. sapiens* (NP\_001013858.1, 718 aa)

**Fig. 3.** Schematic illustration of interactions between SAC and KNL1 in animals/yeasts, plants, and holocentric *Cuscuta* species. Schematics were adapted from refs. 6 and 27, with modifications to reflect the results of other studies cited below. (A) SAC and KNL1 in animals and yeast. (Left) SAC is activated on kinetochores that are not attached to microtubules, and its formation is initiated by MPS1, a kinase that phosphorylates MELT repeats in KNL1. Phosphorylated KNL1 serves as a binding platform for SAC, which interacts with CDC20 to form the mitotic checkpoint complex, preventing entry into anaphase. (Right) Schematic representation of the protein-binding domains in KNL1 [drawn after (28)]. Protein interactions in both schematics are shown as adjacent rectangles or black lines. (B) Domain organization in BUB1/MAD3 family (BMF) proteins in animals/yeasts and their plant counterparts BMF1-BMF3 [drawn after (27)]. (C) SAC and KNL1 in plants. (Left) The architecture of the plant SAC differs from that in animals/yeasts (27, 29, 30, 31), and the function and interactions of some SAC proteins are not yet known (dashed lines with question marks). (Right) Plant KNL1 lacks MELT, KI1, and KI2 domains and binds BMF1 and BMF2 proteins via the BMF domain near the C terminus (29). (D) SAC and KNL1 in holocentric *Cuscuta* species. (Left) SAC is severely impaired by the absence or truncation of several proteins (white and gray boxes, respectively). (Right) Truncation of KNL1 in *Cuscuta* species as compared to *I. nil*. The region missing in the monocentric *Cuscuta* species corresponds to a highly variable region (V), whereas the region missing in the holocentric species also includes a segment that shares sequence similarity to KNL1 from various plant species (S). The truncations are depicted as dotted lines, and their lengths are indicated by the numbers below. (E) Structure of MAD1. N-terminal domain (NTD), MAD2 interaction motif (MIM), and C-terminal domain (CTD) were determined by comparison with human MAD2 (32). C-terminal truncation of MAD2 in holocentric *Cuscuta* species resulted in the loss of domains interacting with MAD2, BUB1, and MPS1 in humans.

(*C* and *E*), demonstrating that they were functional for *in situ* detection. These results suggest that CENH3 is either not present in the chromatin of *C. epithymum* or that its levels are considerably lower than those in *C. europaea*, and thus below the limits of detection for the applied *in situ* immunodetection technique. This was also confirmed using western blot detection of CENH3 in the two holocentric species (*SI Appendix*, Fig. S13*B*). Despite the absence of CENH3 signals,  $\alpha$ -tubulin immunostaining revealed attachment of mitotic spindle microtubules to chromosomes along their poleward sides, confirming the holocentric nature of chromosomes in *C. epithymum* (Fig. 4*C*). This was in contrast to monocentric *Cuscuta* spp., which had microtubules attached only to CENH3-containing domains (Fig. 4*D*). These results suggest

that CENH3 does not function as a foundational kinetochore protein in holocentric *Cuscuta* species.

**Conventional Kinetochore Assembly Is Impaired in Holocentric *Cuscuta* Species.** The chromosomal distribution of CENH3 together with the truncation of three structural kinetochore proteins suggested that kinetochore assembly may be impaired in holocentric *Cuscuta* species. To test whether the kinetochore assembles along the poleward chromosome surface, as expected for holocentric chromosomes, we examined the localization of CENP-C, which is a linker between CENH3 and the KMN network, and of MIS12, KNL1, and NDC80, which represent the three complexes of the KMN network (Fig. 1*B*). Antibodies were developed against peptides

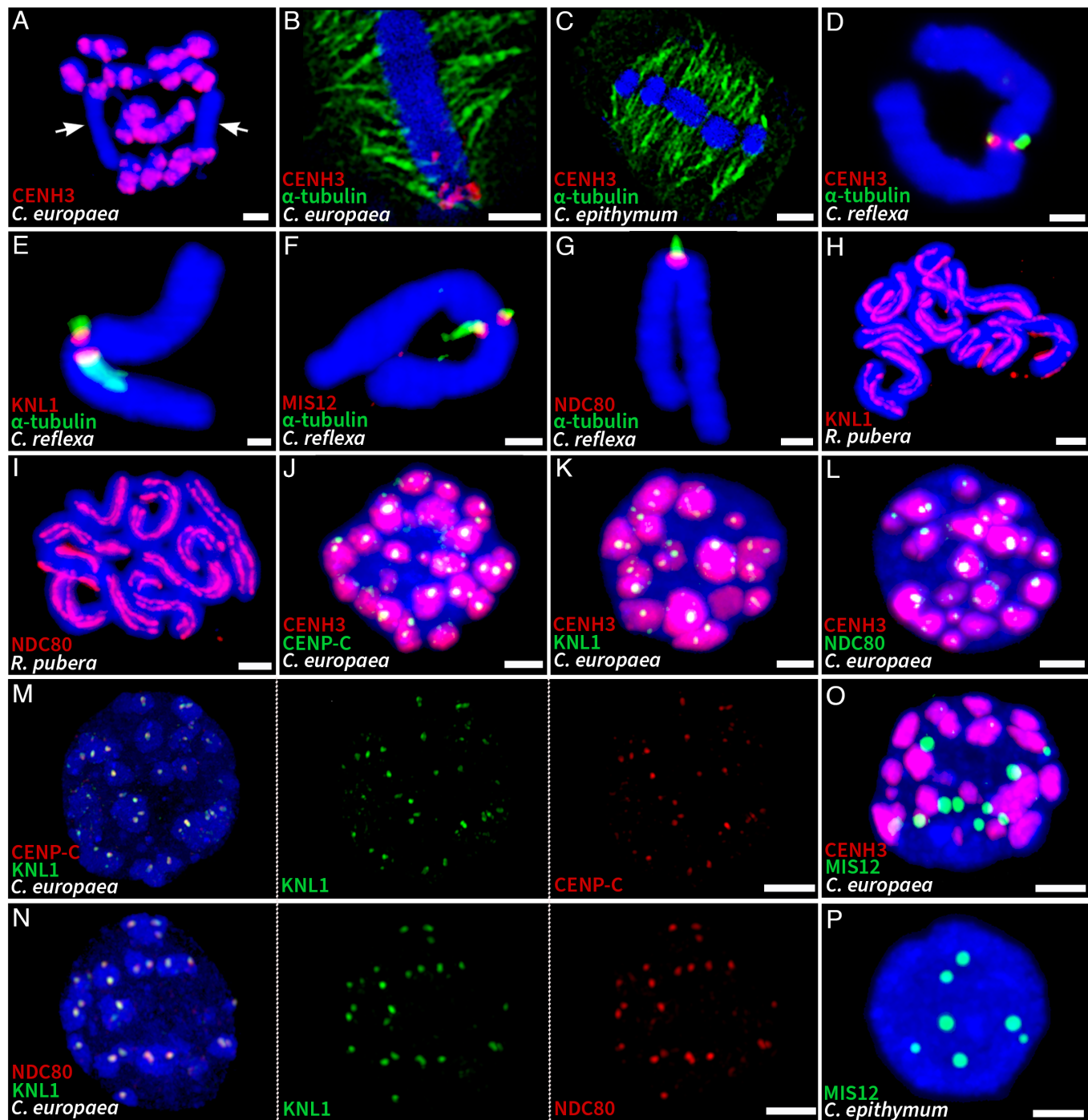


**Fig. 4.** In situ immunodetection of structural kinetochore proteins and  $\alpha$ -tubulin. (A) Detection of CENH3 on mitotic chromosomes in *C. europaea*. Arrows indicate chromosomes 1, which possess a single subtelomeric CENH3-containing domain, while the majority of the chromosome lacks CENH3 signals. (B) Detection of CENH3 and  $\alpha$ -tubulin on selected chromosome 1 in *C. europaea*. The image is a single optical section selected from a 3D-SIM image stack showing that microtubules of the mitotic spindle are evenly attached to the chromosome at its poleward sides and along its entire length, independent of the occurrence of CENH3 signals. (C) Detection of CENH3 and  $\alpha$ -tubulin in *C. epithymum*. The image is a single optical section selected from a 3D-SIM image stack showing an even distribution of microtubules of the mitotic spindle despite the absence of CENH3 signals. (D–G), Detection of  $\alpha$ -tubulin with either CENH3 (D), KNL1 (E), MIS12 (F), or NDC80 (G) on selected *C. reflexa* chromosomes. All the four proteins are specifically localized on the surface of primary constriction where microtubules attach. (H and I) Detection of KNL1 (H) and NDC80 (I) in *R. pubera*. Both proteins show holocentromere-characteristic distribution of both proteins along the entire length of all chromosomes. (J–L) Detection of CENH3 with either CENP-C (J), KNL1 (K), or NDC80 (L) in interphase nuclei of *C. europaea*. CENP-C, KNL1, and NDC80 are localized in small domains embedded in much larger CENH3-containing heterochromatin domains. The images were reconstructed using maximum-intensity projection from 3D-SIM image stacks. (M and N) Detection of KNL1 with either CENP-C (M) or NDC80 (N), showing that all the three proteins are colocalized. The images were reconstructed using maximum-intensity projection from 3D-SIM image stacks. (O) Detection of MIS12 and CENH3 in an interphase nucleus of *C. europaea*. Note that the signals detected by the two antibodies do not overlap. (P) Detection of MIS12 in the interphase nucleus of *C. epithymum*. The spatial visualizations of nuclei shown in K, M, N, and O are available in Movies S1–S4. Chromosomes were stained with DAPI (blue). (Scale bar, 2  $\mu$ m.)

designed from domains that were conserved in the holocentric species. However, owing to the high sequence similarity between species, it was likely that the antibodies against KNL1, NDC80, and

MIS12 would also recognize homologous proteins from monocentric *Cuscuta* species. Indeed, when these antibodies were used for in situ detection, monocentromeres in *C. australis* as well as in *C.*

*reflexa* from the more distant subgenus *Monogynella* were labeled, demonstrating the functionality of the antibodies (Fig. 4 E–G and *SI Appendix*, Fig. S14). The antibodies against KNL1 and NDC80 proved to be particularly versatile, functioning even in *Rhynchospora pubera*, an evolutionarily very distant plant species with holocentric chromosomes, where they detected holocentromere-characteristic signals for both proteins (Fig. 4 H and I). In agreement with the lack of CENH3 signal in *C. epithymum*, CENP-C, KNL1, and NDC80 were not detected on either mitotic chromosomes or in interphase nuclei in this species (*SI Appendix*, Fig. S12). In *C. europaea*, these three proteins were detected in small subdomains embedded within CENH3-containing heterochromatin during interphase but not on mitotic chromosomes (Fig. 4 J–L, *SI Appendix*, Fig. S15, and Movie S1). Simultaneous in situ detection of KNL1 with either CENP-C or NDC80 revealed that these proteins fully colocalized (Fig. 4 M and N and Movies S2 and S3). These results suggest that the assembly of the kinetochore during interphase in *C. europaea* still depends, at least in part, on the presence of CENH3, but that kinetochore organization is disrupted before cells enter mitosis. Strikingly, 2 to 16 (n = 100) discrete spots were labeled with the MIS12 antibody in the interphase nuclei of both holocentric species (Fig. 4 O and P). In *C. europaea*, these spots were always located away from the CENH3-containing heterochromatin (Fig. 4O and Movie S4), suggesting the absence or depletion of MIS12 in domains that contain CENP-C, KNL1, and NDC80. No signals were detected with the MIS12 antibody on mitotic chromosomes in either holocentric *Cuscuta* species (*SI Appendix*, Fig. S16).

#### Conventional SAC Is Abolished in Holocentric *Cuscuta* Species.

To test whether the regulatory kinetochore complexes form on chromosomes in holocentric *Cuscuta* species despite the absence of the tested kinetochore proteins and the massive loss of the SAC genes observed, we raised antibodies against BUB3;1/2 and Borealin, which are components of the SAC and CPC, respectively. While the BUB3;1/2 antibodies produced monocentric-like signals on chromosomes in *C. reflexa*, and holocentromere-like signals in *R. pubera*, BUB3;1/2 was not detectable on chromosomes in holocentric *Cuscuta* species (Fig. 5 A and B). On the contrary, the antibodies against Borealin labeled the chromosomes in the region around areas of sister chromatid cohesion at centromeres in monocentric *C. reflexa* and along the entire chromosome length in both holocentric *Cuscuta* species (Fig. 5 C–E). These results indicate that the conventional SAC is abolished, while the CPC maintains at least some of its functions in holocentric *Cuscuta* species.

## Discussion

The peculiar CENH3 localization in *C. europaea* described in our previous study (15) suggested that the transition to holocentricity in the genus *Cuscuta* may have been associated with the formation of a CENH3-independent kinetochore assembly. In this study, we have demonstrated that the transition to holocentricity in *Cuscuta* species was associated with extensive changes in structural and regulatory kinetochore protein genes, and disruption of both standard kinetochore assembly and SAC regulation of mitotic chromosome segregation. This distinguishes holocentric *Cuscuta* species from both the holocentric nematode *Caenorhabditis elegans*, which uses the CENH3–CENP-C pathway of kinetochore assembly (36), and holocentric insects, in which the CENH3–CENP-C pathway of kinetochore assembly was lost and replaced by the CENP-T pathway (12–14) (Fig. 6).

We hypothesize that one of the most important changes in the evolution of holocentric *Cuscuta* species was the loss of KNL2. In *C. elegans*, RNAi depletion of KNL2 leads to a reduction in the

presence of CENH3 to levels undetectable by immunodetection, resulting in chromosome segregation defects and embryonic lethality (33, 34). Similar phenotypes have been observed in KNL2 mutants in other species, including *A. thaliana*, demonstrating the general importance of KNL2 for CENH3 loading (25, 35). Therefore, the depletion/absence of CENH3 in *C. epithymum* chromatin could be due to the absence of both KNL2 variants. On the contrary, it is puzzling that CENH3 accumulates in heterochromatin domains in *C. europaea* despite the loss of KNL2. Given that all heterochromatin domains that contain CENH3 possess the same repetitive sequences, whereas the heterochromatin domain that lacks these repeats also lacks CENH3 (15, 37), the incorporation of CENH3 into these domains could be DNA sequence dependent. In light of the importance of KNL2 and CENH3 for centromere determination and kinetochore assembly, it is surprising that the loss of KNL2 in both holocentric *Cuscuta* species, the depletion/absence of CENH3 on chromosomes in *C. epithymum*, and the peculiar CENH3 distribution on chromosomes in *C. europaea* are neither lethal nor cause chromosome segregation defects. The simplest explanation is that CENH3 is no longer necessary for correct chromosome segregation in holocentric *Cuscuta* species (*SI Appendix*, Fig. S17).

The absence of detectable levels of structural kinetochore proteins on mitotic chromosomes in holocentric *Cuscuta* species is in contrast not only to monocentric *Cuscuta* species but also to the holocentric-like distribution of NDC80 and KNL1 in *R. pubera* (Cyperaceae), which was used as a holocentric control plant in this study (Fig. 4). This suggests that the formation of the standard kinetochore is disrupted in holocentric *Cuscuta* species. In *C. epithymum*, this could be primarily a direct consequence of the depletion/absence of CENH3 on the chromosomes. In *C. europaea*, the causes of kinetochore disruption must be different because CENH3-containing heterochromatin is present throughout the cell cycle and partially colocalizes with CENP-C, KNL1, and NDC80 proteins during interphase. The reasons why the putative complex of kinetochore proteins formed during interphase disappears at the onset of mitosis are not clear. Considering that three structural kinetochore proteins are truncated (Fig. 1A), one possibility is that the complex falls apart because of disrupted interactions between kinetochore components (Fig. 1C). We hypothesize that the N-terminal truncation of CENP-C may play an important role because CENP-C is the only protein known to link centromeric chromatin to the outer kinetochore in plants (Figs. 1 B and C and 2A). Although the N terminus of CENP-C is divergent in sequence between eukaryotes, it has been shown to bind MIS12c in both humans and yeast, indicating a conserved function (18, 38, 39). Given that this function is also conserved in plants, the N-terminal truncation of CENP-C in *C. europaea* should interfere with MIS12c binding. Consistent with this notion, the MIS12 antibody did not detect signals in CENH3-containing domains, suggesting that MIS12 is absent or depleted in domains containing CENP-C, KNL1, and NDC80 (Fig. 4O and Movie S4). Because we cannot rule out the possibility that the MIS12 antibody cross-reacts with other proteins, further evidence is needed to confirm that the signals in discrete CENH3-lacking domains are indeed due to MIS12 accumulation. While the colocalization of CENP-C, KNL1, and NDC80 suggests that the kinetochore assembles during interphase, despite the absence of MIS12, the complex may not be sufficiently stable to survive mitosis. The N-terminal truncation of CENP-C is, however, unlikely to cause the disappearance of the protein itself because the N terminus is not required for the binding of centromeric nucleosomes (Fig. 2A and 4O). Although the internal portion of CENP-C contains a domain that binds centromeric nucleosomes in

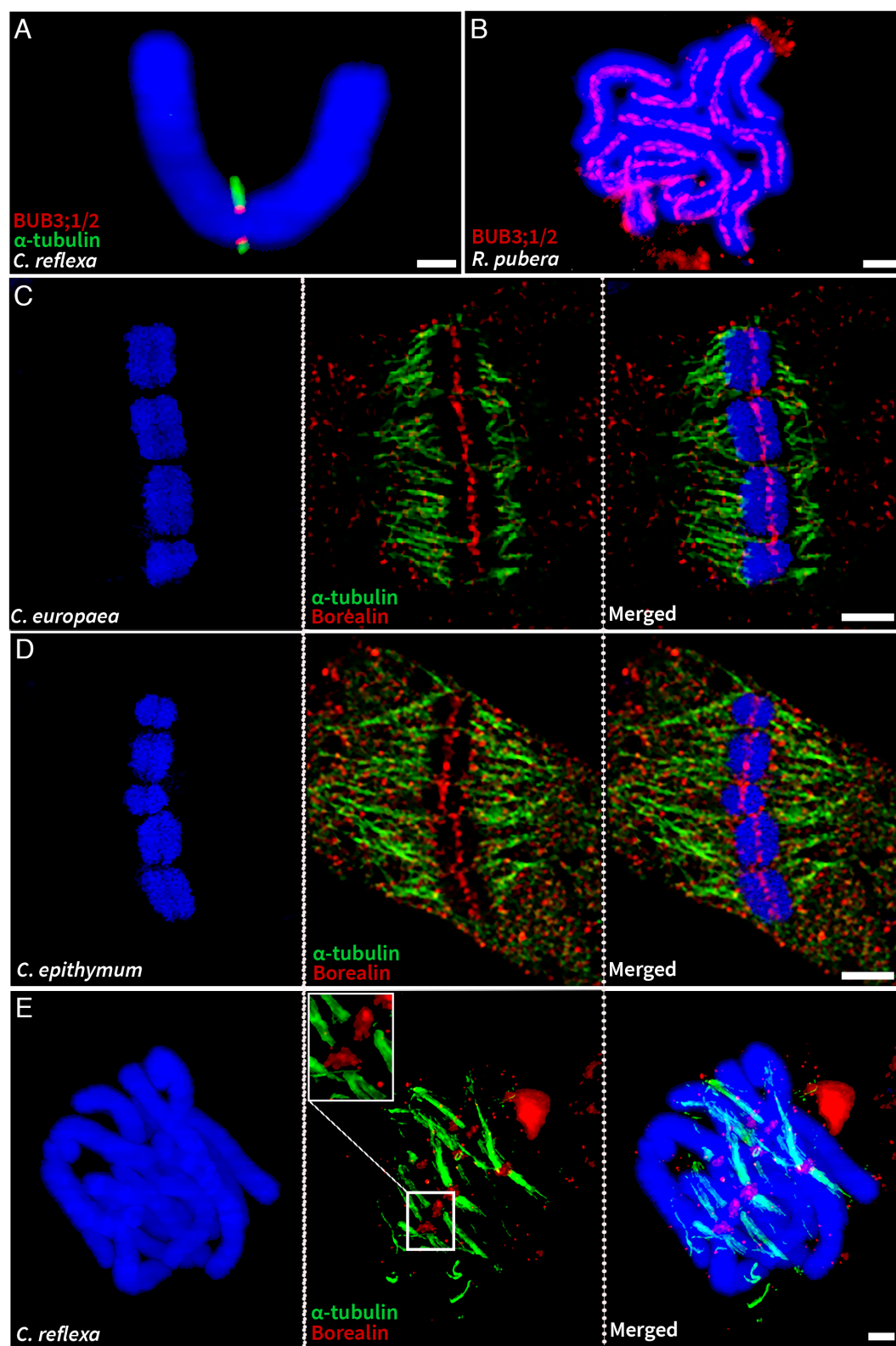


**Fig. 5.** In situ immunodetection of BUB3;1/2 and Borealin. (A) Simultaneous detection of BUB3;1/2 and  $\alpha$ -tubulin on mitotic chromosomes in *C. reflexa*. The image shows that BUB3;1/2 is specifically localized on the surface of the primary constriction where microtubules attach. (B) Detection of BUB3;1/2 on mitotic chromosomes in *R. pubera*, showing holocentromere-characteristic distribution of the signals along the entire length of all chromosomes. (C and D) Simultaneous detection of Borealin and  $\alpha$ -tubulin on mitotic chromosomes in *C. europaea* (C) and *C. epithymum* (D). The images show single optical slices selected from 3D-SIM image stacks. (E) Simultaneous detection of Borealin and  $\alpha$ -tubulin on mitotic chromosomes in *C. reflexa*. Chromosomes were stained with DAPI (blue). (Scale bar, 2  $\mu$ m.)

humans and yeast (Fig. 2*A*), the high sequence divergence of CENP-C prevented us from determining by a sequence similarity-based approach whether it overlaps with the region lost in *C. europaea*. On the contrary, the large size disparity between

the domains containing CENH3 and CENP-C (Fig. 4*J* and *M* and [Movies S1](#) and [S2](#)) suggests that there is an imbalance between the levels of the two proteins that may reflect inefficient binding of CENP-C to CENH3.

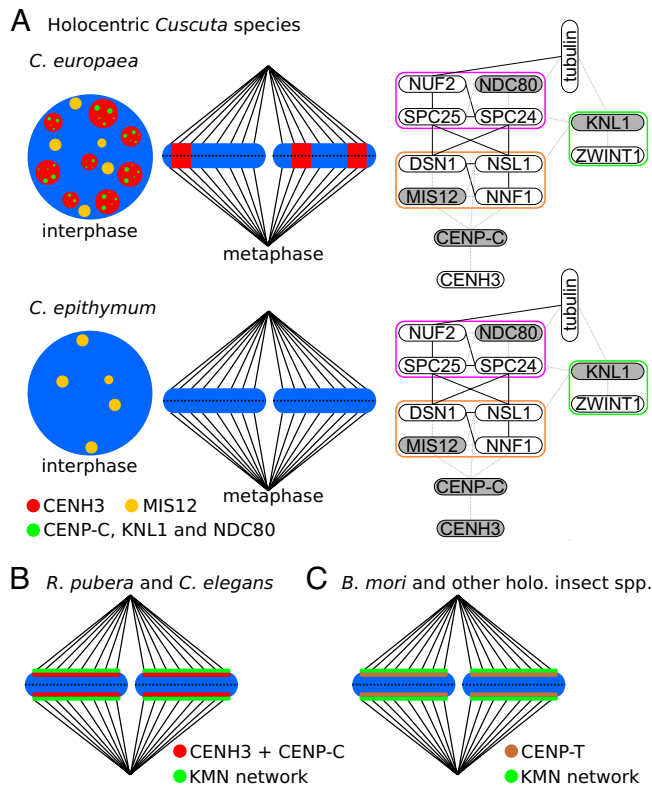


**Fig. 6.** Comparison of kinetochore structure between holocentric *Cuscuta* species and other previously studied holocentric species. (A) (Left) Summary of the results of in situ immunodetection of structural kinetochore proteins examined in this study in *C. europaea* and *C. epithymum*. In both *Cuscuta* species, the microtubules of the mitotic spindle are attached to the chromosomes along their entire length, indicating their holocentric nature. In *C. europaea*, CENH3 is specifically localized in transverse heterochromatin bands rather than on the poleward surface along the entire chromosome length. During interphase, the kinetochore proteins CENP-C, KNL1, and NDC80 are colocalized in small areas within CENH3-containing heterochromatin. None of these proteins were detected on mitotic chromosomes. In *C. epithymum*, which lacks conspicuous heterochromatin domains, CENH3, CENP-C, KNL1, and NDC80 were not detected in interphase nuclei or on mitotic chromosomes. In both species, MIS12 antibody labeled several discrete sites in interphase nuclei, which were always separated from CENH3-containing heterochromatin in *C. europaea*. (Right) Schematic illustrations of the interactions between the proteins forming the CENP-C pathway of kinetochore assembly from Fig. 1C, where the proteins that were examined but not detected on mitotic chromosomes are shaded in gray and the resulting missing interactions are shown as gray dashed lines. They show that the absence of these proteins likely disrupts overall kinetochore assembly. (B) Kinetochore formation on holocentromeres in *R. pubera* and *Caenorhabditis elegans*. Centromere domains are determined by the presence of CENH3. On mitotic chromosomes, they form a continuous layer on the poleward surface of each chromatid where the kinetochore forms and spindle microtubules attach. The KMN network of the outer kinetochore is connected to the CENH3-containing nucleosomes via the CENP-C protein. (C) Kinetochore formation on holocentromeres in *Bombyx mori* and other holocentric insect species. These species lack CENH3 and the KMN network is linked to chromosomes via the CENP-T protein.

The results discussed above support a model in which holocentric *Cuscuta* species either use substantially reduced kinetochores lacking CENH3, CENP-C, KNL1, MIS12, and NDC80 or, more likely, have evolved a completely unique mechanism of chromosome attachment to the mitotic spindle. This conclusion is also supported by the degeneracy of SAC genes that would have been required had the kinetochore been present and functioning in a conventional manner. The absence of detectable amounts of KNL1, NDC80, and MIS12 on metaphase chromosomes distinguishes holocentric *Cuscuta* species from holocentric insects in which kinetochores lack CENH3 and CENP-C but have a complete KMN network connected to centromeric chromatin via CENP-T (12, 14). Although

the existence of CENP-T in plants cannot be ruled out, it is unlikely that the potential presence of CENP-T in holocentric *Cuscuta* species could compensate for the absence/depletion of CENP-C and KMN proteins on mitotic chromosomes, unless the hypothetical CENP-T protein evolved to connect centromeric chromatin and microtubules either directly or via interaction with other proteins. Alternative kinetochores have already been described in Kinetoplastida, most of which have lost CENH3 and all CCAN and KMN genes. They consist of proteins that probably evolved from meiotic components of chromosome synapsis and homologous recombination machinery (41, 42). Moreover, kinetochore-independent chromosomal movement along the spindle, facilitated by kinesin motor proteins, has been described for acentric chromosomes in *Drosophila* neuroblasts (43, 44) and for chromatin knobs in maize (45, 46).

Given that all holocentric *Cuscuta* species are limited to the subgenus *Cuscuta*, while monocentric species belong to either the sister subgenus *Grammica* or the evolutionarily more distant subgenus *Monogynella*, holocentricity in the genus *Cuscuta* has probably a monophyletic origin. Although *C. europaea* and *C. epithymum* diverged only 1.2 to 3.2 Mya, the subgenus *Cuscuta* is much older, having evolved 16.6 to 17.5 Mya (*SI Appendix*, Fig. S10 and 16). Therefore, studying only two closely related holocentric *Cuscuta* species can only provide limited insight into the evolution of holocentricity. In this regard, it will be particularly intriguing to identify changes shared by all holocentric *Cuscuta* species, as these may have played a crucial role in the transition to holocentricity.

Overall, we have shown that the transition to holocentricity in *Cuscuta* species was unique among all species studied to date. It was accompanied, and perhaps even triggered, by the degeneration of standard kinetochore structure and regulation and the formation of a unique mechanism for chromosome attachment to microtubules. The insights gained in this study provide the basis for future studies aimed at uncovering the plasticity of kinetochore assembly and discovering yet unknown principles of chromosome segregation.

## Material and Methods

**Plant Material.** Seeds of *C. europaea* (serial number: 0101147) were obtained from the Royal Botanic Gardens (Ardingly, UK). *C. epithymum* plants were collected from a natural population at "U Cáby" (Kroclov, Czech Republic). Seeds of *C. australis* and *C. campestris* were provided by Prof. Jianqiang Wu (Kunming Institute of Botany, Chinese Academy of Sciences, Kunming, China) and Dr. Chnar Fathoulla (University of Salahaddin, Kurdistan Region, Iraq), respectively. *C. reflexa* Roxb. plant was obtained from the Botanic Gardens of the Rhenish Friedrich-Wilhelm University (Bonn, Germany). *Cuscuta* plants were cultivated on the following host plant species: *Urtica dioica* (*C. europaea*), *Betonica officinalis* and *Coleus blumei* (*C. epithymum*), *Ocimum basilicum* (*C. australis* and *C. campestris*), or *Pelargonium zonale* (*C. reflexa*). Plants of *R. pubera* were obtained from Dr. André Marques (Max Planck Institute for Plant Breeding Research, Cologne, Germany).

**Genome Sequencing and Assembly.** DNA for Illumina and Pac-Bio sequencing was isolated using the CTAB method from nuclei extracted from young shoots of *C. europaea* and *C. epithymum* as described previously (47). Shotgun Illumina paired-end sequencing of DNA was performed by the Brigham Young University (Provo, UT, USA) and Admira Health (South Plainfield, NJ, USA). High-molecular-weight nuclear DNA used for Oxford nanopore sequencing was isolated using a modified CTAB protocol as described previously (48). Nanopore sequencing was performed as described (37). Detailed information about all genome sequence datasets produced in this study is provided in *SI Appendix*, Table S4.

Illumina paired-end reads and Oxford nanopore reads were assembled using MaSuRCA (49). PacBio HiFi reads were assembled using Hifiasm assembler [v0.15.5-r350; (50)] with default parameters for PacBio HiFi sequence reads. Since the quality of the HiFi-based assemblies was considerably better than those generated by MaSuRCA (*SI Appendix*, Table S1), they were selected for submission to European Nucleotide Archive (<https://www.ebi.ac.uk/ena/browser/home>; accession numbers: GCA\_945859875 (*C. europaea*) and GCA\_945859915

(*C. epithymum*). Completeness and contiguity of assemblies were evaluated using BUSCO [v5.2.2; (51)] and QUAST [v5.0.2; (52)]. Genome characteristics were evaluated using kmer analysis and the jellyfish program (53) with kmer lengths 21 and 51 for Illumina and PacBio HiFi sequence reads, respectively. Heterozygosity was estimated using GenomeScope program (54).

**Transcriptome Sequencing, Assembly, and Gene Prediction.** Total RNA was isolated using the Trizol method. Preliminary sequencing for de-novo transcriptome assemblies of *C. epithymum*, *C. europaea*, and *C. campestris* was performed at GATC Biotech (Konstanz, Germany) using Illumina technology producing 50 bp paired-end reads. In each species, RNA was isolated from shoots and inflorescences, mixed in a 1:1 ratio, treated with DNase I (Ambion, Austin, TX, USA), and then enriched for poly-A fraction using the Dynabeads mRNA purification kit (Thermo Fisher Scientific, Waltham, MA, USA). Deep transcriptome sequencing of *C. epithymum*, *C. europaea*, and *C. australis* was done using RNA isolated from shoot tips, shoot internodia, or inflorescences at various stages of development. For each species and tissue, the RNA samples were produced in three biological replicates (samples from different plants collected at different times). Subtraction of poly-A RNA using NEBNext Ultra II with a Poly-A Selection kit (New England Biolabs, Ipswich, MA, USA) and poly-A RNA sequencing were performed at Admera Health (South Plainfield, NJ, USA). The sequencing generated more than 500 million 151 nt-long paired-end reads for each RNA sample, giving a total yield of about 5 billion reads per species (*SI Appendix*, Table S5).

Transcriptomes were de-novo assembled using the Trinity program (55) with default options from paired-end reads. Sequences from individual replicates and tissue samples of each species were concatenated before their assembly. The presence of single-copy orthologs in the transcriptomes was evaluated using the BUSCO (v5.2.2) program (51). To create gene models, paired-end RNA-Seq Illumina reads were aligned to genome assembly using the STAR program [v2.7.7a; (56)] with parameters -outSAMstrandField intronMotif -outSAMtype BAM SortedByCoordinate -alignIntronMax 20000. Each sample was aligned independently. Resulting alignments were merged into a single BAM file using samtools (57). Whole-length transcripts and genes were then reconstructed using the StringTie program [v2.1.7; (58)] with parameters -c 2 -f 0.05. Candidate coding regions within transcript sequences were identified using TransDecoder program (<https://github.com/TransDecoder/TransDecoder>) with default settings.

Predicted protein sequences from *C. europaea* and *C. epithymum* were compared with published proteomes of *C. campestris*, *C. australis*, and *Ipomoea nil* using program OrthoFinder [v2.5.2; (59)] to identify orthologs and orthogroups. Genome assemblies and associated files containing detailed information about predicted gene models, protein, and CDS sequences were downloaded from <http://plabipd.de/portal/cuscuta-campestris> (*C. campestris*) or GenBank (<https://www.ncbi.nlm.nih.gov/genbank/>; *C. australis*: GCA\_003260385.1; *I. nil*: GCF\_001879475.1). RNA-Seq data for these species were downloaded from the Sequence Read Archive (SRA; <https://www.ncbi.nlm.nih.gov/sra>) from the following accession numbers: SRR6664647-SRR6664654 (*C. australis*), ERR1916345-ERR1916364 (*C. campestris*), and DRR024544-DRR024549 (*I. nil*). The RNA-Seq data produced in this study or downloaded from other studies were used to verify and correct automatically predicted gene models if needed. Manual verification and editing of gene models were performed using Apollo Genome Annotation Editor (60).

**Identification and Characterization of Kinetochore Proteins.** Structural and regulatory kinetochore protein sequences identified in *A. thaliana* were downloaded from uniprot database and published studies (27, 29, 61). These sequences were used for blastp searches to identify their homologs in genome assemblies of *C. australis* and *C. campestris* (62, 63), representing monocentric *Cuscuta* species, and in *I. nil* (64), selected as a monocentric nonparasitic genus of the family Convolvulaceae. All sequences with significant similarity hits were manually inspected to remove false positives, correct erroneous protein sequences, or add additional variants due to alternative splicing. Protein sequences from *A. thaliana* and the three Convolvulaceae species were combined into a reference dataset that was used for blastp and tblastn searches to find homologous kinetochore protein genes in holocentric *C. epithymum* and *C. europaea*. The searches were primarily performed in gene and protein sequences predicted using StringTie in the assembly produced from Pac-Bio reads, but the results were verified using the data from the parallel genome assemblies that were made from Illumina and nanopore reads as well as the transcriptome assemblies produced using Trinity.

CENH3 sequences from additional *Cuscuta* species or other plants of the same *Cuscuta* species were obtained from our previous study [*C. campestris*, *C. japonica* (15)], identified in transcriptome shotgun assemblies (*C. reflexa*, *C. campestris*) or other available genome assembly (*C. epithymum*), amplified from RNA using RT-PCR or RACE methods (*C. epithymum*), or reconstructed from available next-generation genome sequence data using GRABb and GeneWise programs [*C. americana*, *C. californica*, *C. pentagona*; (65, 66)]. More detailed information about the sources of the CENH3 sequences is provided in *SI Appendix, Table S6*.

Sequence alignments were performed using MUSCLE (67). Time trees were inferred using ITS and *rbcL* sequences and methods described in our previous study (16). ITS and *rbcL* sequences from *C. australis* were reconstructed from Illumina paired-end reads (SRA run accession number: SRR5851367) using RepeatExplorer (68). A search for conserved sequence motives was performed using MEME (69). Sequence logos were generated using WebLogo (70). The sources of CENP-C and ZWINT1 sequences used for MEME and WebLogo analyses are provided in *SI Appendix, Table S7*.

**Antibodies.** Antibodies to all kinetochore proteins used in this study were custom-produced by GenScript (Piscataway, NJ, USA) or Biomatik (Cambridge, ON, Canada) against peptides designed from regions that were most conserved among *Cuscuta* species and *I. nil* (*SI Appendix, Fig. S18* and *Table S8*). Detailed information about the development and validation of the antibodies is provided in *SI Appendix, Supporting text*. The mouse monoclonal antibody to  $\alpha$ -tubulin was purchased from Sigma-Aldrich (St. Louis, MO, USA; catalog number: T6199). Western blot and *in situ* immunodetection techniques are described in *SI Appendix, Supporting text*.

**Microscopy.** For conventional wide-field fluorescence microscopy, a Zeiss AxioImager. Z2 microscope equipped with an AxioCam 506 mono camera was used along with an Apotome2.0 device for better resolution in the z-axis, which was needed when the images were composed of multiple optical sections. Images were generated using the ZEN 3.2 software (Carl Zeiss GmbH). To capture signals at the super-resolution level (~120 nm using a 488-nm laser), spatial structured illumination microscopy (3D-SIM) was performed using a 63 $\times$ /1.4 Oil Plan-ApoChromat objective on an Elyra PS.1 microscope system, controlled by the ZENBlack software (Carl Zeiss GmbH). Images were captured using the 405-, 488-, and 561-nm laser lines for excitation and the appropriate emission filters (71). Three-dimensional movies were produced from 3D-SIM image stacks using the Imaris 9.7 (Bitplane) software.

**Data, Materials, and Software Availability.** Raw DNA/RNA sequence data have been deposited in [<https://www.ebi.ac.uk/ena/browser/home>] (ERR10073826, ERR10073827, ERR5237073, ERR5237074, ERR10739381, ERR10739380, ERR9250942, ERR9250943, ERR10073828, ERR10683985, ERR9250941, ERR9250871, ERR9250872, ERR9250873, ERR9250868, ERR9250869, ERR9250870, ERR9250865, ERR9250867, ERR9250866, ERR9250880, ERR9250881, ERR9250882, ERR9250877, ERR9250878, ERR9250879, ERR9250874, ERR9250875, ERR9250876, ERR9250889, ERR9250890, ERR9250891, ERR9250886, ERR9250887, ERR9250888, ERR9250883, ERR9250884, ERR9250885, ERR3651373, ERR9784846, and ERR3651372) and can be accessed under study accessions PRJEB35300 (72), PRJEB42863 (73), and PRJEB51495 (74). Genome assemblies of *C. europaea* and *C. epithymum* are available in [<https://www.ncbi.nlm.nih.gov/data-hub/genome/>] under accession numbers GCA\_945859875 (75) and GCA\_945859915 (76), respectively.

**ACKNOWLEDGMENTS.** This research was financially supported by grants from the Czech Science Foundation (20-25440S) and the Czech Academy of Sciences (RVO:60077344). Computational resources and data storage facilities were provided by the ELIXIR-CZ Research Infrastructure Project (LM2018131). We thank J. Látalová and V. Tetourová for technical assistance.

Author affiliations: <sup>a</sup>Biology Centre, Czech Academy of Sciences, Institute of Plant Molecular Biology, České Budějovice 37005, Czech Republic; <sup>b</sup>Department of Biological Science, College of Bioscience and Biotechnology, Chungnam National University, Daejeon 34134, Republic of Korea; and <sup>c</sup>Department of Breeding Research, Leibniz Institute of Plant Genetics and Crop Plant Research (IPK) Gatersleben, 06466 Seeland, Germany

Author contributions: P. Neumann, A.H., and J.M. designed research; P. Neumann, L.O., T.-S.J., A.K., and J.M. performed research; V.S. and A.H. contributed new reagents/analytic tools; P. Neumann, L.O., P. Novák, V.S., and J.M. analyzed data; and P. Neumann, L.O., P. Novák, and J.M. wrote the paper.

1. D. P. Melters, L. V. Paliulis, I. F. Korf, S. W. L. Chan, Holocentric chromosomes: Convergent evolution, meiotic adaptations, and genomic analysis. *Chromosome Res.* **20**, 579–93 (2012).
2. K. L. McKinley, I. M. Cheeseman, The molecular basis for centromere identity and function. *Nat. Rev. Mol. Cell Biol.* **17**, 16–29 (2016).
3. M. E. Pesenti, J. R. Weir, A. Musacchio, Progress in the structural and functional characterization of kinetochores. *Curr. Opin. Struct. Biol.* **37**, 152–163 (2016).
4. Y. Yamagishi, T. Sakuno, Y. Goto, Y. Watanabe, Kinetochore composition and its function: Lessons from yeasts. *FEMS Microbiol. Rev.* **38**, 185–200 (2014).
5. P. Lara-Gonzalez, F. G. Westhorpe, S. S. Taylor, The spindle assembly checkpoint. *Curr. Biol.* **22**, R966–R980 (2012).
6. A. Musacchio, The molecular biology of spindle assembly checkpoint signaling dynamics. *Curr. Biol.* **25**, R1002–R1018 (2015).
7. S. Komaki *et al.*, Functional analysis of the plant chromosomal passenger complex. *Plant Physiol.* **183**, 1586–1599 (2020).
8. M. Carmena, M. Wheelock, H. Funabiki, W. C. Earnshaw, The chromosomal passenger complex (CPC): From easy rider to the godfather of mitosis. *Nat. Rev. Mol. Cell Biol.* **13**, 789–803 (2012).
9. M. S. van der Waal, R. C. C. Hengeveld, A. van der Horst, S. M. A. Lens, Cell division control by the chromosomal passenger complex. *Exp. Cell Res.* **318**, 1407–1420 (2012).
10. B. J. Buchwitz, K. Ahmad, L. L. Moore, M. B. Roth, S. Henikoff, A histone-H3-like protein in *C. elegans*. *Nature* **401**, 547–548 (1999).
11. V. Schubert *et al.*, Super-resolution microscopy reveals diversity of plant centromere architecture. *Int. J. Mol. Sci.* **21**, 3488 (2020).
12. N. Cortes-Silva *et al.*, CenH3-independent kinetochore assembly in Lepidoptera requires CCAN, including CENP-T. *Curr. Biol.* **30**, 561–572.e10 (2020).
13. I. A. Drinnenberg, D. DeYoung, S. Henikoff, H. S. Malik, Recurrent loss of CenH3 is associated with independent transitions to holocentricity in insects. *Elife* **3**, e03676 (2014).
14. A. P. Senaratne *et al.*, Formation of the CenH3-deficient holocentromere in Lepidoptera avoids active chromatin. *Curr. Biol.* **31**, 173–181.e7 (2021).
15. L. Oliveira *et al.*, Mitotic spindle attachment to the holocentric chromosomes of *Cuscuta europaea* does not correlate with the distribution of CENH3 chromatin. *Front. Plant Sci.* **10**, 1799 (2020).
16. P. Neumann *et al.*, Impact of parasitic lifestyle and different types of centromere organization on chromosome and genome evolution in the plant genus *Cuscuta*. *New Phytol.* **229**, 2365–2377 (2021).
17. M. Hara, T. Fukagawa, Where is the right path heading from the centromere to spindle microtubules? *Cell Cycle* **18**, 1199–1211 (2019).
18. A. Petrovic *et al.*, Structure of the Mis12 complex and molecular basis of its interaction with CENP-C at human kinetochores. *Cell* **167**, 1028–1040.e15 (2016).
19. C. Ciferrí *et al.*, Implications for kinetochore-microtubule attachment from the structure of an engineered Ndc80 complex. *Cell* **133**, 427–439 (2008).
20. G. M. Alushin *et al.*, The Ndc80 kinetochore complex forms oligomeric arrays along microtubules. *Nature* **467**, 805–810 (2010).
21. J. P. I. Welburn *et al.*, Aurora B phosphorylates spatially distinct targets to differentially regulate the kinetochore-microtubule interface. *Mol. Cell* **38**, 383–392 (2010).
22. A. Petrovic *et al.*, Modular assembly of RWD domains on the Mis12 complex underlies outer kinetochore organization. *Mol. Cell* **53**, 591–605 (2014).
23. R. Valverde, J. Ingram, S. C. Harrison, Conserved tetramer junction in the kinetochore Ndc80 complex. *Cell Rep.* **17**, 1915–1922 (2016).
24. A. Ali-Ahmad, S. Bilokapic, I. B. Schäfer, M. Halić, N. Sekulić, CENP-C unwraps the human CENP-A nucleosome through the H2A C-terminal tail. *EMBO Rep.* **20**, 1–13 (2019).
25. S. Zuo *et al.*, Recurrent plant-specific duplications of KNL2 and its conserved function as a kinetochore assembly factor. *Mol. Biol. Evol.* **39** (2022).
26. P. Hornung *et al.*, A cooperative mechanism drives budding yeast kinetochore assembly downstream of CENP-A. *J. Cell Biol.* **206**, 509–524 (2014).
27. S. Komaki, A. Schnittger, The spindle assembly checkpoint in *Arabidopsis* is rapidly shut off during severe stress. *Dev. Cell* **43**, 172–185.e5 (2017).
28. P. Ghongane, M. Kapanidou, A. Asghar, S. Elowe, V. M. Bolanos-Garcia, The dynamic protein Knl1 - a kinetochore rendezvous. *J. Cell Sci.* **127**, 3415–3423 (2014).
29. H. Su *et al.*, Knl1 participates in spindle assembly checkpoint signaling in maize. *Proc. Natl. Acad. Sci. U.S.A.* **118**, e2022357118 (2021).
30. M. C. Caillaud *et al.*, Spindle assembly checkpoint protein dynamics reveal conserved and unsuspected roles in plant cell division. *PLoS One* **4**, e6757 (2009).
31. H. Zhang *et al.*, Role of the BUB3 protein in phragmoplast microtubule reorganization during cytokinesis. *Nat. Plants* **4**, 485–494 (2018).
32. Y. Luo, E. Ahmad, S.-T. Liu, MAD1: Kinetochore receptors and catalytic mechanisms. *Front. Cell Dev. Biol.* **6**, 1–10 (2018).
33. P. S. Maddox, F. Hyndman, J. Monen, K. Oegema, A. Desai, Functional genomics identifies a Myb domain-containing protein family required for assembly of CENP-A chromatin. *J. Cell Biol.* **176**, 757–763 (2007).
34. F. A. Steiner, S. Henikoff, Holocentromeres are dispersed point centromeres localized at transcription factor hotspots. *Elife* **3**, 1–22 (2014).
35. I. Lermontova *et al.*, *Arabidopsis* KINETOCHERE NULL2 is an upstream component for centromeric histone H3 variant cenH3 deposition at centromeres. *Plant Cell* **25**, 3389–404 (2013).
36. L. Pintard, B. Bowerman, Mitotic cell division in *Caenorhabditis elegans*. *Genetics* **211**, 35–73 (2019).
37. T. Vondrák *et al.*, Complex sequence organization of heterochromatin in the holocentric plant *Cuscuta europaea* elucidated by the computational analysis of nanopore reads. *Comput. Struct. Biotechnol. J.* **19**, 2179–2189 (2021).
38. Y. N. Dimitrova, S. Jenni, R. Valverde, Y. Khin, S. C. Harrison, Structure of the MIND complex defines a regulatory focus for yeast kinetochore assembly. *Cell* **167**, 1014–1027.e12 (2016).
39. E. Scropanti *et al.*, Direct binding of Cenp-C to the Mis12 complex joins the inner and outer kinetochore. *Curr. Biol.* **21**, 391–398 (2011).
40. M. R. Przewloka *et al.*, CENP-C is a structural platform for kinetochore assembly. *Curr. Biol.* **21**, 399–405 (2011).
41. E. C. Tromer, T. A. Wemessy, P. Ludzia, R. F. Waller, B. Akiyoshi, Repurposing of synaptonemal complex proteins for kinetochores in Kinetoplastida. *Open Biol.* **11**, 210049 (2021).
42. A. Butenko *et al.*, Evolution of metabolic capabilities and molecular features of diplomonads, kinetoplastids, and euglenids. *BMC Biol.* **18**, 1–28 (2020).
43. T. Karg, M. W. Elting, H. Vicars, S. Dumont, W. Sullivan, The chromokinesin Klp3a and microtubules facilitate acentric chromosome segregation. *J. Cell Biol.* **216**, 1597–1608 (2017).
44. H. Vicars, T. Karg, B. Warecki, I. Bast, W. Sullivan, Kinetochore-independent mechanisms of sister chromosome separation. *PLOS Genet.* **17**, e1009304 (2021).
45. K. W. Swentowsky *et al.*, Distinct kinesin motors drive two types of maize neocentromeres. *Genes Dev.* **34**, 1239–1251 (2020).
46. R. K. Dawe *et al.*, A Kinesin-14 motor activates neocentromeres to promote meiotic drive in maize. *Cell* **173**, 839–850 (2018).
47. S. L. Dellaporta, J. Wood, J. B. Hicks, A plant DNA minipreparation: Version II. *Plant Mol. Biol. Rep.* **1**, 19–21 (1983).
48. T. Vondrák *et al.*, Characterization of repeat arrays in ultra-long nanopore reads reveals frequent origin of satellite DNA from retrotransposon-derived tandem repeats. *Plant J.* **101**, 484–500 (2020).
49. A. V. Zimin *et al.*, The MaSuRCA genome assembler. *Bioinformatics* **29**, 2669–2677 (2013).
50. H. Cheng, G. T. Concepcion, X. Feng, H. Zhang, H. Li, Haplotype-resolved de novo assembly using phased assembly graphs with hifiasm. *Nat. Methods* **18**, 170–175 (2021).
51. M. Manni, M. R. Berkeley, M. Seppey, F. A. Simão, E. M. Zdobnov, BUSCO update: Novel and streamlined workflows along with broader and deeper phylogenetic coverage for scoring of eukaryotic, prokaryotic, and viral genomes. *Mol. Biol. Evol.* **38**, 4647–4654 (2021).
52. A. Gurevich, V. Saveliev, N. Vyahhi, G. Tesler, QUAST: Quality assessment tool for genome assemblies. *Bioinformatics* **29**, 1072–1075 (2013).
53. G. Marçais, C. Kingsford, A fast, lock-free approach for efficient parallel counting of occurrences of k-mers. *Bioinformatics* **27**, 764–770 (2011).
54. G. W. Vurture *et al.*, GenomeScope: Fast reference-free genome profiling from short reads. *Bioinformatics* **33**, 2202–2204 (2017).
55. M. G. Grabherr *et al.*, Full-length transcriptome assembly from RNA-Seq data without a reference genome. *Nat. Biotechnol.* **29**, 644–652 (2011).
56. A. Dobin *et al.*, STAR: Ultrafast universal RNA-seq aligner. *Bioinformatics* **29**, 15–21 (2013).
57. H. Li *et al.*, The sequence alignment/map format and SAMtools. *Bioinformatics* **25**, 2078–2079 (2009).
58. M. Pertea *et al.*, StringTie enables improved reconstruction of a transcriptome from RNA-seq reads. *Nat. Biotechnol.* **33**, 290–295 (2015).
59. D. M. Emms, S. Kelly, OrthoFinder: Phylogenetic orthology inference for comparative genomics. *Genome Biol.* **20**, 1–14 (2019).
60. N. A. Dunn *et al.*, Apollo: Democratizing genome annotation. *PLOS Comput. Biol.* **15**, e1006790 (2019).
61. J. J. van Hooff, E. Tromer, L. M. van Wijk, B. Snel, G. J. Kops, Evolutionary dynamics of the kinetochore network in eukaryotes as revealed by comparative genomics. *EMBO Rep.* **18**, 1559–1571 (2017).
62. G. Sun *et al.*, Large-scale gene losses underlie the genome evolution of parasitic plant *Cuscuta australis*. *Nat. Commun.* **9**, 2683 (2018).
63. A. Vogel *et al.*, Footprints of parasitism in the genome of the parasitic flowering plant *Cuscuta campestris*. *Nat. Commun.* **9**, 2515 (2018).
64. A. Hoshino *et al.*, Genome sequence and analysis of the Japanese morning glory *Ipomoea nil*. *Nat. Commun.* **7**, 13295 (2016).
65. B. Brankovics *et al.*, GRAB: Selective assembly of genomic regions, a new niche for genomic research. *PLoS Comput. Biol.* **12**, e1004753 (2016).
66. E. Birney, M. Clamp, R. Durbin, Genewise and genomewise. *Genome Res.* **14**, 988–995 (2004).
67. R. C. Edgar, MUSCLE: Multiple sequence alignment with high accuracy and high throughput. *Nucleic Acids Res.* **32**, 1792–1797 (2004).
68. P. Novák, P. Neumann, J. Macas, Global analysis of repetitive DNA from unassembled sequence reads using RepeatExplorer2. *Nat. Protoc.* **15**, 3745–3776 (2020).
69. T. L. Bailey, C. Elkan, Fitting a mixture model by expectation maximization to discover motifs in biopolymers. *Proc. Int. Conf. Intell. Syst. Mol. Biol.* **2**, 28–36 (1994).
70. G. E. Crooks, G. Hon, J.-M. Chandonia, S. E. Brenner, WebLogo: A sequence logo generator. *Genome Res.* **14**, 1188–1190 (2004).
71. K. Weisshart, J. Fuchs, V. Schubert, Structured illumination microscopy (SIM) and photoactivated localization microscopy (PALM) to analyze the abundance and distribution of RNA polymerase II molecules on flow-sorted *Arabidopsis* nuclei. *Bio-protocol* **6**, 1–32 (2016).
72. P. Neumann, P. Novák, J. Macas, Project PRJEB35300: Characterization of transcriptomes in *Cuscuta* spp. European Nucleotide Archive. <https://www.ebi.ac.uk/ena/browser/view/PRJEB35300>. Deposited 8 November 2019.
73. J. Macas, P. Novák, P. Neumann, Project PRJEB42863: Genome sequencing of *Cuscuta europaea*. European Nucleotide Archive. <https://www.ebi.ac.uk/ena/browser/view/PRJEB42863>. Deposited 3 February 2021.
74. P. Neumann, P. Novák, J. Macas, Project PRJEB51495: Investigation of changes associated with the formation of holocentric chromosomes in *Cuscuta* spp. European Nucleotide Archive. <https://www.ebi.ac.uk/ena/browser/view/PRJEB51495>. Deposited 9 March 2022.
75. P. Novák, P. Neumann, J. Macas, Submitted GenBank sequence GCA\_945859875.1: Genome assembly of *Cuscuta europaea*. NCBI Datasets. [https://www.ncbi.nlm.nih.gov/data-hub/genome/GCA\\_945859875.1/](https://www.ncbi.nlm.nih.gov/data-hub/genome/GCA_945859875.1/). Deposited 27 November 2022.
76. P. Novák, P. Neumann, J. Macas, Submitted GenBank sequence GCA\_945859915.1: Genome assembly of *Cuscuta epithymum*. NCBI Datasets. [https://www.ncbi.nlm.nih.gov/data-hub/genome/GCA\\_945859915.1/](https://www.ncbi.nlm.nih.gov/data-hub/genome/GCA_945859915.1/). Deposited 27 November 2022.